Sensors & Transducers, Vol. 248, Issue 1, January 2021, pp. 10-17

www.sensorsportal.com

Sensors & Transducers

Published by IFSA Publishing, S. L., 2021
http://www.sensorsportal.com

Modelling Spontaneous Ca^{2+} Oscillations Using a Digital Astrocyte System Based on Single-Electron Transistors

[1, *] Beatriz O. CÂMARA and [2] Janaína G. GUIMARÃES

[1] University of Brasilia, Electrical Engineering Department, P.O. Box 4368, Brasília, Brazil
[2] Federal University of Santa Catarina, Department of Control Engineering, Automation and Computer Science, Rua João Pessoa 2750, 89036-256, Velha, Blumenau, Brazil
E-mail: bia.camara@gmail.com

Received: 2 November 2020 /Accepted: 12 December 2020 /Published: 29 January 2021

Abstract: This work presents an improved version of a digital nanoelectronic astrocyte. This module simulates the spontaneous Ca^{2+} oscillations in the cytosol. Ca^{2+} oscillations are often initiated by *stimuli* from neighboring neurons, but they can also be triggered by small calcium ions flow from the external environment into the astrocyte's cytosol. The hardware presented is a single-electron transistor-based model with a reduced footprint in relation to other digital astrocytes that implement the same model, and it generates the spontaneous oscillations without great loss of precision.

Keywords: Single-electron Transistor, Nanoelectronics, Neuromorphic Systems, Astrocyte, Neural Networks.

1. Introduction

Artificial Neural Networks (ANN) are a highly popular method of machine learning [1–3]. The deep learning algorithm specifically has brought on varied interest to the area, fuelling the research in this subject [2, 4]. New processing units and overpowered graphics processing units (GPU) have also greatly contributed to the increase in ANNs popularity, making it possible to process big data and to run networks with thousands of neurons and synapses. However, even the great processing power available on new computers cannot surpass their main issue in relation to ANNs: the von Neumann architecture [2, 5].

Seeking to overcome this problem Carver Mead created the notion of neuromorphic systems on his seminal paper [5]. A neuromorphic system has a hardware architecture inspired on the nervous system, making it a natural fit for ANNs. Neurons and synapses are distributed in a hardware with highly parallel connections. The neuromorphic circuit occupies a much smaller area, dissipates less power, and provides higher speeds. Big companies are already producing neuromorphic processors, such as *Intel* with *Intel Loihi* [6], and *IBM* with *True North* [7]. Neuromorphic systems bring new ANN implementation possibilities and was voted as one of the top ten emerging technologies by the World Economic Forum in 2015 [8].

Despite its great success, ANNs are built upon the premise that all the cognitive function in central nervous system is processed by the neurons alone. Research dating back to the 1990s show, however, that the astrocytes play an active part in cognition [9]. This glial cell was once thought of as being a passive structural element. Recent experimental results show that astrocytes have a significant role in neural spike synchronization, synaptic transmission, and information processing. They are directly involved in

synapse regulation, through the tripartite synapse [10], [11], and are active participants in learning and memory through the calcium oscillations.

While all the mechanisms involved in these processes are still unknown, some of them are well understood, as shown in mathematical models like the *Li-Rinzel* model [12], the *Postnov* model [13], and the *DePittà* model [14]. These models cover the tripartite synapse, the Ca^{2+} oscillations that are triggered by neuron activity, and the oscillations modulation in AM, FM, and AFM. *Lavrentovich, et al.* [15] proposes a mathematical model for spontaneous oscillations, which are *stimuli* independent. Unlike the other referred models, there are few works that implement the spontaneous oscillations model, either as algorithms or neuromorphic systems. Currently there are only two neuromorphic implementations of this model [16, 17].

The hardware implementation of astrocytes is a first step to create a fully integrated neuron-astrocyte neuromorphic circuit. This works improves a previously implemented digital spontaneous astrocyte module.

2. Spontaneous Oscillations Model

While most Ca^{2+} oscillations events in astrocytes are a result of external stimulation, they can also be formed spontaneously. The spontaneous oscillations model is a mathematical model proposed by *Lavrentovich, et al.* [15], which seeks to describe this process.

The spontaneous oscillations are triggered by small changes in the cytosolic Ca^{2+} concentrations and is sustained by the interactions between the IP_3 and the extracellular, cytosolic, and endoplasmic Ca^{2+} concentrations. No other external influence is needed to trigger this behavior. The oscillation mechanism relies on two feedback loops.

The first loop (Fig. 1) describes the IP_3 production mechanisms and its relation to the release of Ca^{2+} from the endoplasmic reticulum (ER). As calcium ions flows from outside of the astrocyte to its cytosol through the cellular membrane, the Ca^{2+} concentration in the cytosol ($[Ca^{2+}]_{cyt}$) increases. The $[Ca^{2+}]_{cyt}$ positively influences the activation process of the delta-form of phospholipase C (PLCδ1), which is responsible by the production of IP_3. IP_3 is a known key intracellular messenger, and it binds to IP_3 receptors (IP_3R) on the membrane of the ER causing the release of Ca^{2+} from the ER into the cytosol. As the $[Ca^{2+}]_{cyt}$ changes, so does the production IP_3, completing this feedback loop.

The second loop (Fig. 2) centers on the IP_3R binding mechanism with Ca^{2+}. Calcium ions are also able to bind to the ER receptors and they can positively or negatively feedback on ER's Ca^{2+} liberation. At lower concentrations in the cytosol, Ca^{2+} ions activate the opening of IP_3R, increasing the Ca^{2+} flow from the ER to the cytosol. At higher concentrations Ca^{2+} ions have an inhibitory effect. Coupled with that there is the Ca^{2+} sequestration through the sarco(endo)plasmic calcium (SERCA) pumps. The complete spontaneous oscillations mechanism is shown in Fig. 3. The + and – signals on the images depicts an increase or decrease in the cytosolic calcium ions' concentration.

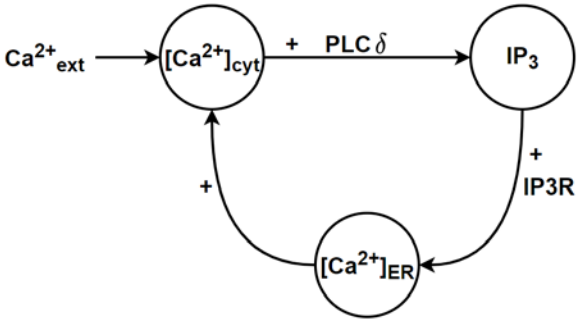

Fig. 1. The first feedback loop that is centered around the inositol cross-coupling (ICC) mechanism. The external Ca^{2+} enters the astrocyte's cytosol, increasing the calcium ion concentration. This increase positively influences the production of IP_3 through the PLCδ. The IP_3 in turn binds to the receptors in the ER, causing the release of more Ca^{2+} into the cytosol.

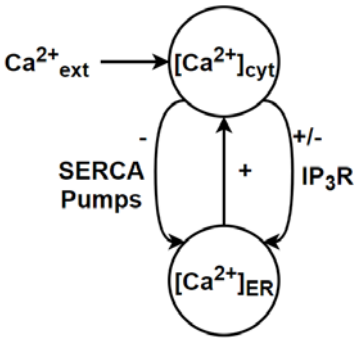

Fig. 2. The second feedback loop focus on the calcium-induced calcium-release (CICR) mechanism. The calcium ions also interact with the IP3R and modulates the ER calcium release through it. The increase in the Ca^{2+} concentration in the cytosol inhibits this release. At the same time the ions in the cytosol are sequestered into the ER by the SERCA pumps.

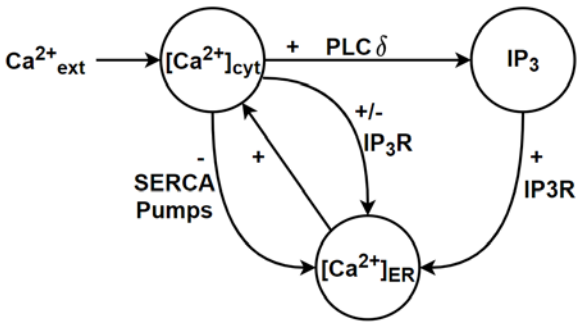

Fig. 3. The complete spontaneous oscillation mechanism shows the interplay between the three main variables in this model. Both ICC and CICR mechanisms act together to create the calcium oscillations.

The model is described by a system of three differential equations, where X= $[Ca^{2+}]_{cyt}$, Y= $[Ca^{2+}]_{ER}$ and Z= $[IP_3]_{cyt}$.

$$\frac{dX}{dt} = V_{in} - k_{out}X + V_{CICR} - V_{SERCA} + k_f(Y - X), \quad (1)$$

$$\frac{dY}{dt} = V_{SERCA} - V_{CICR} - k_f(Y - X), \quad (2)$$

$$\frac{dZ}{dt} = V_{PLC} - k_{deg}Z, \quad (3)$$

$$V_{SERCA} = V_{M2}\left(\frac{X^2}{X^2 + {k_2}^2}\right), \quad (4)$$

$$V_{PLC} = V_p\left(\frac{X^2}{X^2 + {k_p}^2}\right), \quad (5)$$

$$V_{CICR} = 4V_{M3}\left(\frac{{k_{CaA}}^n X^n}{(X^n + {k_{CaA}}^n)(X^n + {k_{CaI}}^n)}\right) \times \left(\frac{Z^m}{Z^m + {k_{ip3}}^m}\right)(Y - X) \quad (6)$$

The parameters description is as follow:

- V_{in}: represents the flow of calcium from the extracellular space through the astrocyte's membrane into the cytosol.
- $k_{out}X$: rate of calcium efflux from the cytosol into the extracellular space.
- V_{CICR}: represents the IP_3R mediated flux of calcium from the ER into the cytosol.
- V_{SERCA}: describes the sarco(endo)plasmic reticulum ATPase that fills the ER with Ca^{2+} from the cytosol.
- $k_f(Y-X)$: represents the leak flux from the ER into the cytosol due to the concentration gradient.
- V_{PLC}: represents the IP_3 production due to the PLCδ1 activation.
- $k_{deg}Z$: represents the degradation of IP_3, based on the linear dependence of IP_3 degradation by 5-phosphatase.
- V_{M2}: maximum flux of calcium ions out of the SERCA pump.
- k_2: V_{SERCA} fix factor.
- V_{M3}: maximum flux of Ca^{2+} into the cytosol.
- k_{CaA}: activating affinity of IP_3R-2 (type-2 isoform).
- k_{CaI}: inhibiting affinity of IP_3R-2.
- k_{ip3}: IP_3 factor.
- n, m: Hill coefficient.

The parameter values employed in the original paper are listed in Table 1. They are also the values employed in this work.

Despite being exhibited in Table 1 as a fixed value, V_{in} is a variable that changes the external influence over the oscillation process, i.e., it represents the amount of Ca^{2+} entering the astrocyte from the outside of the cell. As we change V_{in} values, so does change the oscillations profile.

V_{in} also indirectly represents the inhibition of PKC. The influx of external Ca^{2+} is indirectly related to the concentration of PKC, which inhibits the Ca^{2+} oscillations. Values for V_{in} higher than 0.07 μM/s, as the other parameters are kept constant, fail to produce the oscillations. Fig. 4 displays the plot for variable X, i.e., the oscillations of Ca^{2+} concentration in the cytosol, for V_{in} values of 0.04, 0.05, 0.06 and 0.08 μM/s. As the values raise so does the frequency of the oscillations, until the PKC concentration becomes high enough to inhibit them. These plots were obtained by using MATLAB ODE [18] solver. The initial conditions applied were: X = 0.1 μM, Y = 1.5 μM and Z = 0.1 μM [15].

Table 1. Spontaneous oscillations model's parameters.

Parameter	Values
$\mathbf{V_{M2}}$	15.0 μM/s
$\mathbf{V_{M3}}$	40.0 s^{-1}
$\mathbf{V_{in}}$	0.05 μM/s
$\mathbf{V_p}$	0.05 μM/s
$\mathbf{k_2}$	0.1 μM
$\mathbf{k_{CaA}}$	0.15 μM
$\mathbf{k_{CaI}}$	0.15 μM
$\mathbf{k_{ip3}}$	0.1 μM
$\mathbf{k_p}$	0.3 μM
$\mathbf{k_{deg}}$	0.08 s^{-1}
$\mathbf{k_{out}}$	0.5 s^{-1}
$\mathbf{k_f}$	0.5 s^{-1}
n	2.02
m	2.2

3. 2D Spontaneous Oscillations Model

The 2D spontaneous oscillations model was proposed by *Haghiri, et al.* [16]. This model aims to reduce the number of variables of the original model from 3 to 2, thus eliminating one differential equation. This model also eliminates multiplications and divisions and exchanges the main nonlinear terms by piecewise linear functions.

These modifications allow faster execution on digital systems and reduce the hardware costs.

Because parameter Z has fast dynamics in comparison with parameters X and Y, and rapidly reaches a steady state, Eq. (3) can be solved for Z as Eq. (7):

$$\frac{dZ}{dt} = 0 \rightarrow Z = \frac{V_{PLC}}{k_{deg}} \quad (7)$$

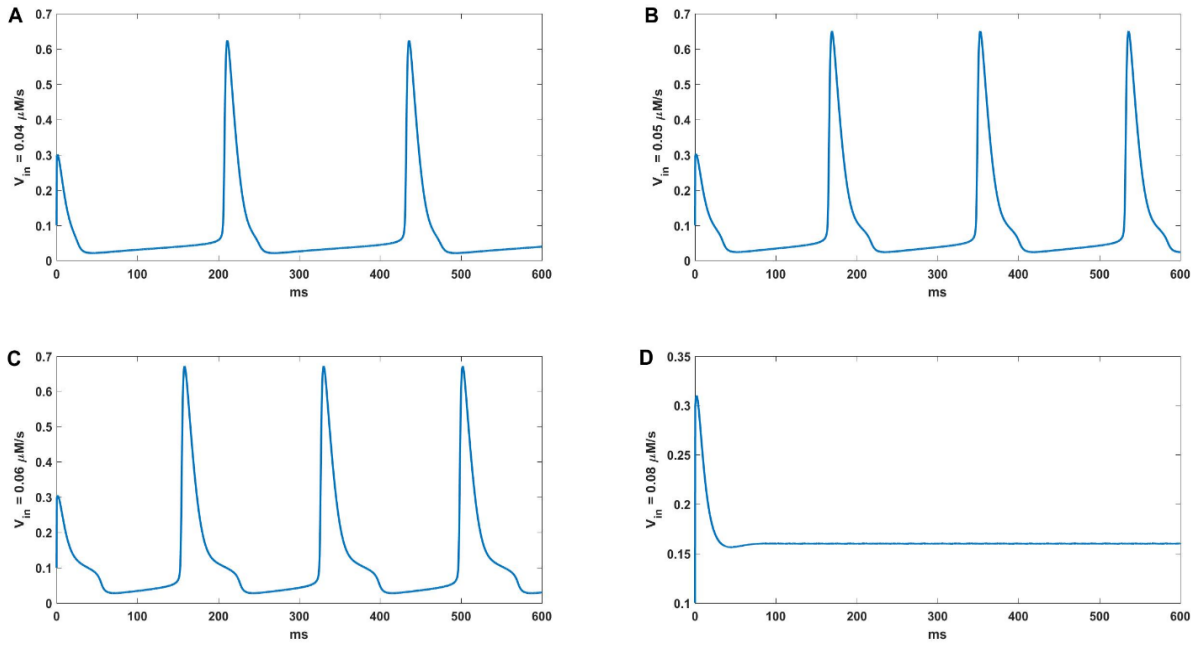

Fig. 4. Spontaneous Ca^{2+} oscillations for various V_{in} values. Pane A shows the oscillations for V_{in} = 0.04 μM. As the values increase to 0.05 μM and 0.06 μM in panes B and C, respectively, so does the frequency. However, at V_{in} = 0.08 μM (pane D) and greater values, there are no more oscillations due to the inhibition from the PKC.

The modified 2D model is now given by Eq. (8) to Eq. (12):

$$\frac{dX}{dt} = V_{in} - k_{out}X + V_{CICR} - V_{SERCA} + k_f(Y - X) \tag{8}$$

$$\frac{dY}{dt} = V_{SERCA} - V_{CICR} - k_f(Y - X) \tag{9}$$

$$V_{SERCA} = V_{M2}\left(\frac{X^2}{X^2 + k_2{}^2}\right) \tag{10}$$

$$V_{CICR} = V_{CC}(Y - X) \tag{11}$$

$$V_{CC} = 4V_{M3}\left[\frac{K_{CaA}^n X^n}{(X^n + K_{CaA}^n)(X^n + K_{CaI}^n)}\right] \times \left[\frac{\left(\frac{V_{PLC}}{K_{deg}}\right)^m}{\left(\frac{V_{PLC}}{K_{deg}}\right)^m + K_{ip3}^m}\right] \tag{12}$$

The piecewise linear function versions of V_{SERCA} and V_{CC} are presented in Eq. (13) and Eq. (14):

$$V_{SERCA} = \begin{cases} 89X - 1.4 & 0 < X < 0.10 \\ 44X + 3.3 & 0.10 < X < 0.20 \\ 15X + 9.1 & 0.20 < X < 0.30 \\ 5.2X + 12 & 0.30 < X < 0.45 \\ 1.6X + 13.55 & else \end{cases} \tag{13}$$

$$V_{CC} = \begin{cases} 0 & 0 < X < 0.04 \\ 35X - 1.4 & 0.04 < X < 0.06 \\ 130X - 7.2 & 0.06 < X < 0.08 \\ 210X - 11 & 0.08 < X < 0.20 \\ -67X + 44 & 0.20 < X < 0.50 \\ -25X + 24 & else \end{cases} \tag{14}$$

Finally, Eq. (8), Eq. (9), Eq. (13) and Eq. (14) must be discretized to achieve a digital implementation. The discretized form of these equations is given by:

$$X[i+1] = dt[V_{in} - k_{out}X[i] + V_{CC}[i]Y[i] - V_{SERCA}[i] + k_f(Y[i] - X[i])] \tag{15}$$

$$Y[i+1] = Y[i] - dt[-V_{SERCA}[i] + V_{CC}[i]Y[i] + k_f(Y[i] - X[i])] \tag{16}$$

$$V_{SERCA}[i] = \begin{cases} 89X[i] - 1.4 & 0 < X[i] < 0.10 \\ 44X[i] + 3.3 & 0.10 < X[i] < 0.20 \\ 15X[i] + 9.1 & 0.20 < X[i] < 0.30 \\ 5.2X[i] + 12 & 0.30 < X[i] < 0.45 \\ 1.6X[i] + 13.55 & else \end{cases} \tag{17}$$

$$V_{CC}[i] = \begin{cases} 0 & 0 < X[i] < 0.04 \\ 35X[i] - 1.4 & 0.04 < X[i] < 0.06 \\ 130X[i] - 7.2 & 0.06 < X[i] < 0.08 \\ 210X[i] - 11 & 0.08 < X[i] < 0.20 \\ -67X[i] + 44 & 0.20 < X[i] < 0.50 \\ -25X[i] + 24 & else \end{cases} \tag{18}$$

4. Single-Electron Transistor

The single-electron transistor (SET) consists of two tunnel junctions connected to create an isolated charge island between them (Fig. 5) [19–23]. A current flow event only happens through charge tunneling across a junction. In a SET the island is small enough that its energy levels are well discretized, and only a discrete number of electrons can accumulate in it. A tunneling event occurs when a potential difference is applied across the double-junctions, which bends the energy band diagram in the island, allowing an electron to tunnel onto it [20].

The gate terminal, which is coupled to the island through an ideal gate capacitance, allows for extra control over the double-tunnel junction. Voltage applied to the gate changes the Fermi level on the island, therefore modifying the necessary voltage through the double-tunnel junctions required to drive a current.

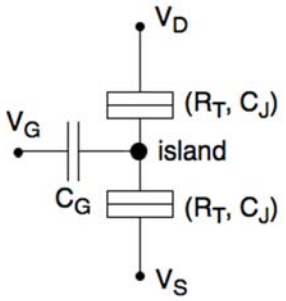

Fig. 5. Schematic for the single-electron transistor. The tunnel junctions can be modeled by a resistance (R_T) together with a capacitance (C_J).

These characteristics offer a high density, high-speed, low-power dissipation device, which are very alluring properties for neuromorphic computation. One of the greatest problems of this device is the low temperature required for its operation. However, SETs that operate up to 350 K are already possible, as reported by *Lavieville, et al.* [22], *Jalil, et al.* [24] and *Katkar, et al.* [25]. The module developed in this work employs a SET SPICE model, which operates at room temperature. This model is proposed by, and is available at, *Lientsching, et al.*[26].

5. SET-Based NAND Logic Gate

Both the NAND and NOR Boolean functions have the functional completeness property, i.e., any Boolean expression can be rewritten using only the NAND (or NOR) operation. Based on this property all logic gates, circuits and modules in this work were designed using only SET-based NAND gates.

Different circuit architectures of SET-based NANDs can be found in the literature. The programmable single-electron NAND/NOR gate presented by *Gerousis, et al.* [21] (Fig. 6) has been deeply analyzed by *Tsiolakis, et al.* [27] and showed stability and energy efficiency, which are interesting parameters for large scale circuits.

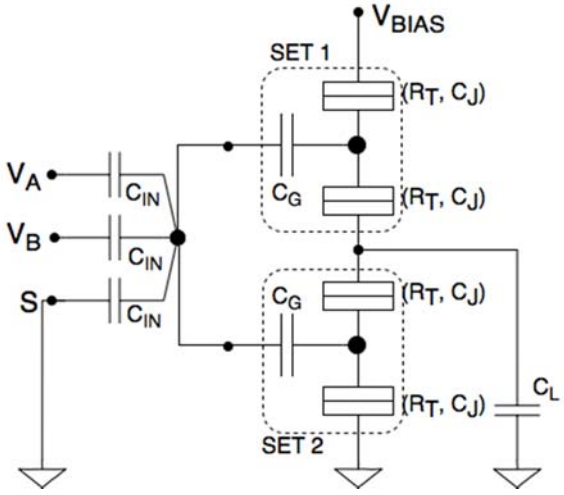

Fig. 6. Programmable SET NAND/NOR gate.

As shown in Fig. 6 voltages V_A and V_B are the gate's inputs A and B, respectively. Voltage S is a select input that enables either the NOR function on the gate's output when its value is high or the NAND function when its value is low. In this work both SETs in the circuit are considered equal (SET1=SET2). The circuit parameters for the designed SET-based NAND are shown in Table 2.

Table 2. SET-based NAND circuit values for room-temperature operation.

Circuit Parameter	Value
C_j	0.01 aF
R_T	1 MΩ
C_g	0.15 aF
C_{in}	2 aF
C_L	0.2 aF
V_{bias}	0.5 V
V_A	0 V (low) and 0.5 V (high)
V_B	0 V (low) and 0.5 V (high)
S	0 V

6. Digital Astrocyte Model

During the development of a digital hardware that intends to simulate an analogical process, one must take into consideration the number of bits that will be assigned to this system. The original digital astrocyte model, proposed by *Haghiri, et al.* [28], was built to work with 41 bits total. 20 of those bits were assigned to the integer part of the numbers, and 20 were assigned to the decimal part. The final bit is used as

the sign of variables and parameters values. However, only 7 of the integer bits and 6 of the decimal bits are used as bit precision. The extra bits are used as overflow bits to the shift operation.

A previously proposed nanoelectronic astrocyte model [17] works with 21 bits. In this new proposal the total number of bits has been reduced to 18 bits, where 7 bits are assigned to the integer part, 6 bits are assigned for the decimal part, 4 bits are overflow bits, and 1 bit is used as value sign.

The digital astrocyte is made of three main units: Main Computing Unit (MCU), Variable Computing Unit (VCU), and Variable Storage Unit (VSU) (Fig. 7). These units' description is as follow:

- **VSU:** this unit is made of two nanoelectronic SRAM [29], one to store the computed values for the variable X, and the other to store values for Y. The VSU memory is readable by all the other units but can only be written by the VCU.

- **VCU:** the VCU is responsible for calculating the next value for both X and Y. There are two separate modules in the VCU, one that computes Eq. (15) for the X variable, and another that computes Eq. (16) for the Y variable. The new values that are obtained are stored in appropriate module in the VSU. Eq. (15) and Eq. (16) use the previous values of the variables (X[i] and Y[i]) to compute the new values (X[i+1] and Y[i+1]). To achieve that the VCU fetches the previous values from the VSU. The computing of X[i+1] also requires the input of variable Vin. As this variable may be changed it is stored separately in a register.

- **MCU:** the MCU computes the values for V_{SERCA} (Eq. 17) and V_{CC} (Eq. 18). The module retrieves the value of X[i] and decides which equation of the equations' system (Eq. (13) and Eq. (14)) to compute based on this value. This decision is made in a comparator that selects the right equation through a MUX. V_{SERCA} and V_{CC} are computed in separate modules and their computed values are forwarded to the VCU module. The MCU activity is controlled by a counter module that is used to synchronize the entire astrocyte circuit and is the trigger to the computing of the next X and Y values.

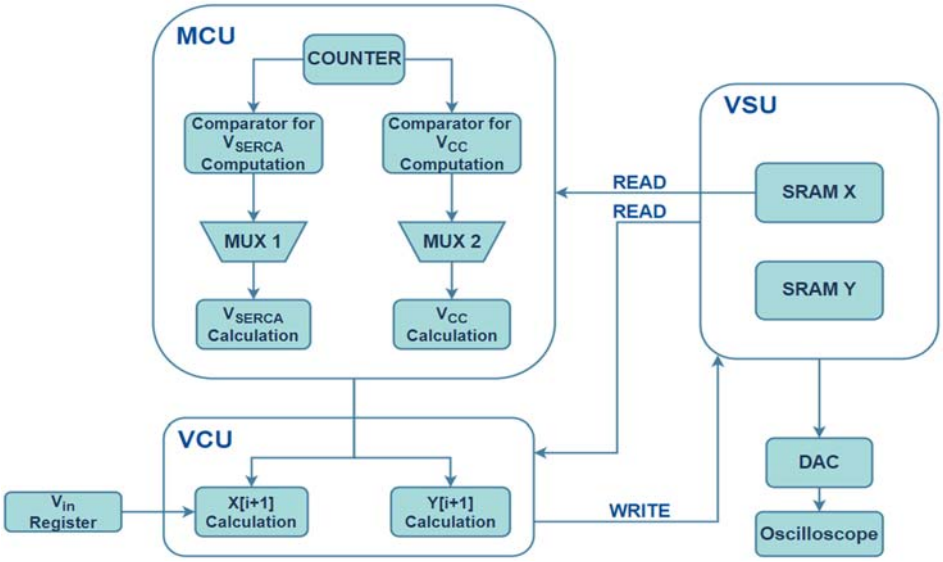

Fig. 7. Digital astrocyte block diagram. The astrocyte is made of three main processing blocks: Main Computing Unit (MCU), Variable Storage Unit (VSU), and Variable Computing Unit (VCU).

7. Results and Discussion

The digital astrocyte simulations were executed on *LTspiceXVII* software [30]. On the beginning of operations the values X[0]=0.1 μM and Y[0]=1.5 μM are stored in binary form on the VSU. These values are the same initial condition values used on the simulation of the original system of differential equations (Eq. (1-3) on *MATLAB*.

The obtained oscillation is displayed on Fig. 8. These oscillations are a close match to those presented in Haghiri, *et al.* [28], and they are also similar enough to the ones obtained in the original model (Fig. 4). The frequencies are maintained and valleys and peaks correspond to the ones on *Lavretovich, et al.* [15]. Despite the reduction in total bits available on the system, a good accuracy is maintained.

However, the system does lose accuracy for values of V_{in} greater than 0.07 μM. Accordingly to the original mathematical model, these values should cause a lack of oscillations due to the inhibitory action of PKC. The piecewise linear functions proposed by *Haghiri, et al.* [16] still generate oscillations as an answer for Vin>0.06 μM. The functional significance of the spontaneous oscillations is still unknown, though it appears that it helps correlate the activity of astrocytes and neurons. Whatever maybe the case this neuromorphic implementation is step further in the direction of a fully integrated astrocyte-neuron network.

Finally, the developed nanoelectronic model has 9.1 μm^2 of area and dissipates 184.8 nW of power. Overall there has been a reduction of about 11 % in occupied area and 12 % of dissipated power, without compromising the accuracy seen on the previous system [17].

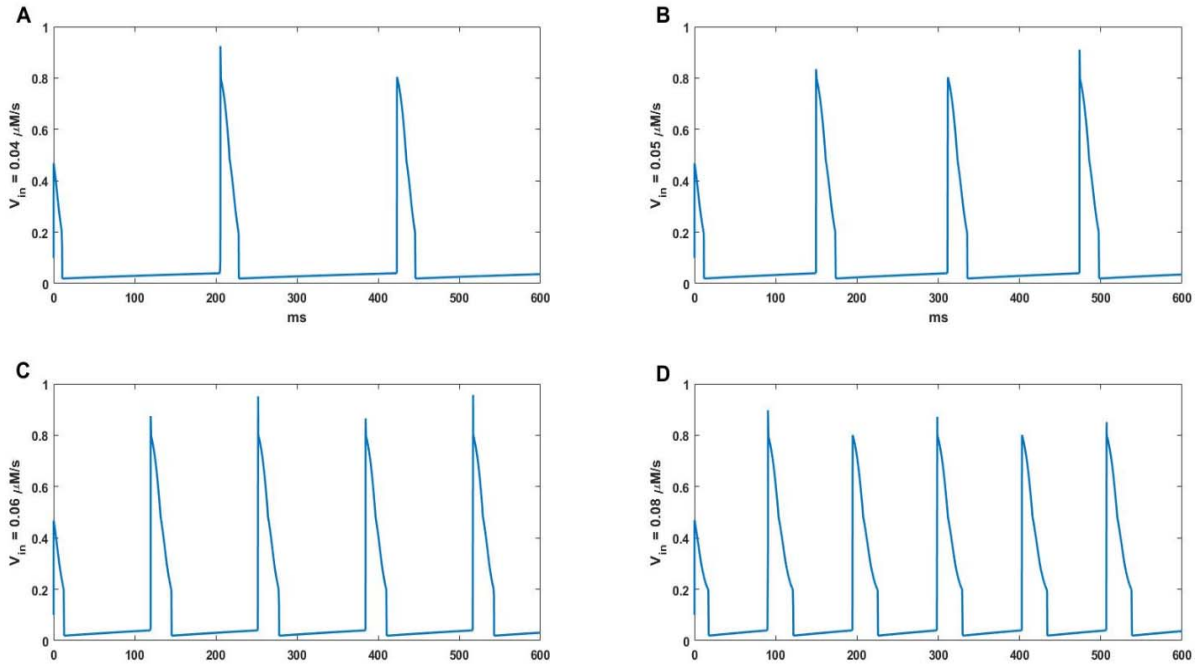

Fig. 8. Ca^{2+} oscillations obtained through LTspice simulation of the digital astrocyte module developed. Panes A, B, C and D show oscillations for V_{in} values of 0.04 μM, 0.05 μM, 0.06 μM and 0.08 μM. Panes A, B and C look remarkably like the original models' oscillations. However, pane D display an inconsistency between the two models.

8. Conclusions

The astrocyte is an important glial cell that not only provides support to the brain but is also involved in the cognition processes such as learning, memory, and adaptation. Recent research provides the mathematical basis upon which to build network systems. The future of artificial neural networks will include the participation of astrocytes.

This work proposed an improved neuromorphic nanoelectronic digital system. The system implements the spontaneous Ca^{2+} oscillations feature and is a functional module ready to be implemented in a network. Future works aim to integrate the astrocyte module with integrate-and-fire neurons to create a hybrid network.

Acknowledgements

This study was financed in part by the Coordenação de Aperfeiçoamento de Pessoal de Nível Superior – Brasil (CAPES) – Finance Code 001. J. G. Guimarães thanks PQ/CNPq for support.

References

[1]. S. Haykin, S. S. Haykin, Neural Networks: A Comprehensive Foundation, *Macmillan College Publishing Company*, 1994.

[2]. A. Basu, *et al.*, Low-Power, Adaptive Neuromorphic Systems: Recent Progress and Future Directions, *IEEE Journal on Emerging and Selected Topics in Circuits and Systems*, Vol. 8, Issue 1, 2018, pp. 6–27.

[3]. E. Alpaydin, Introduction to machine learning, *MIT Press*, 2014.

[4]. I. Goodfellow, Y. Bengio, A. Courville, Deep Learning, *MIT Press*, 2016.

[5]. C. Mead, Neuromorphic electronic systems, *Proc. IEEE*, Vol. 78, Issue 10, 1990, pp. 1629–1636.

[6]. M. Davies, *et al.*, Loihi: A Neuromorphic Manycore Processor with On-Chip Learning, *IEEE Micro*, Vol. 38, Issue 1, 2018, pp. 82–99.

[7]. J. Hsu, IBM's new brain [News], *IEEE Spectrum*, Vol. 51, Issue 10, 2014, pp. 17–19.

[8]. World Economic Forum's Meta-Council on E. Technologies, Top 10 Emerging Technologies of 2015, 12 March 2015.

[9]. A. Volterra, J. Meldolesi, Astrocytes, from brain glue to communication elements: the revolution continues, *Nat. Rev. Neurosci.*, Vol. 6, Issue 8, 2005, pp. 626-640.

[10]. A. Araque, V. Parpura, R. P. Sanzgiri, P. G. Haydon, Tripartite synapses: glia, the unacknowledged partner, *Trends Neurosci.*, Vol. 22, Issue 5, 1999, pp. 208–215.

[11]. M. Heidarpur, P. Khosravifar, A. Ahmadi, M. Ahmadi, CORDIC-Astrocyte: Tripartite Glutamate-IP3-Ca2+ Interaction Dynamics on FPGA, *IEEE Trans. Biomed. Circuits Syst.*, Vol. 14, Issue 1, 2020, pp. 36–47.

[12]. Y. X. Li, J. Rinzel, Equations for InsP3 receptor-mediated [Ca2+](i) oscillations derived from a detailed kinetic model: A hodgkin-huxley like

formalism, *J. Theor. Biol.*, Vol. 166, Issue 4, February 1994, pp. 461–473.
[13]. D. E. Postnov, L. S. Ryazanova, O. V. Sosnovtseva, Functional modeling of neural-glial interaction, *BioSystems*, Vol. 89, Issue 1–3, May 2007, pp. 84–91.
[14]. M. De Pittà, V. Volman, H. Levine, G. Pioggia, D. de rossi, E. Ben-Jacob, Coexistence of amplitude and frequency modulations in intracellular calcium dynamics, *Phys. Rev. E*, Vol. 77, 2008, p. 30903.
[15]. M. Lavrentovich, S. Hemkin, A mathematical model of spontaneous calcium(II) oscillations in astrocytes, *J. Theor. Biol.*, Vol. 251, Issue 4, Apr. 2008, pp. 553–560.
[16]. S. Haghiri, A. Ahmadi, Digital FPGA implementation of spontaneous astrocyte signalling, *Int. J. Circuit Theory Appl.*, p. cta. 2745, Jan. 2020.
[17]. B. O. Câmara, J. G. Guimarães, Digital Single-electron Astrocyte Signaling Implementation, in *Proceedings of the 3rd International Conference on Microelectronic Devices and Technologies (MicDAT'2020)*, 22-23 October 2020, p. 14-17.
[18]. MATLAB - MathWorks - MATLAB & Simulink. [Online]. Available: https://www.mathworks.com/products/matlab.html. [Accessed: 19-Dec-2020].
[19]. G. W. Hanson, Fundamentals of nanoelectronics, *Pearson/Prentice Hall*, 2008.
[20]. D. V. Averin, K. K. Likharev, Coulomb blockade of single-electron tunneling, and coherent oscillations in small tunnel junctions, *J. Low Temp. Phys.*, Vol. 62, Issue 3–4, Feb. 1986, pp. 345–373.
[21]. C. P. Gerousis, S. M. Goodnick, W. Porod, Nanoelectronic single-electron transistor circuits and architectures, *Int. J. Circuit Theory Appl.*, Vol. 32, Issue 5, Sep. 2004, pp. 323–338.
[22]. R. Lavieville, S. Barraud, A. Corna, X. Jehl, M. Sanquer, M. Vinet, 350K operating silicon nanowire single electron/hole transistors scaled down to 3.4 nm diameter and 10 nm gate length, in *Proceedings of the Joint International EUROSOI Workshop and International Conference on Ultimate Integration on Silicon (EUROSOI-ULIS'2015)*, 2015, pp. 9–12.
[23]. K. K. Likharev, Single-electron devices and their applications, *Proc. IEEE*, Vol. 87, Issue 4, Apr. 1999, pp. 606–632.
[24]. J. Jalil, Y. Ruan, Y. Zhu, Room-temperature sensing of single electrons using vibrating-reed electrometer in silicon-on-glass technology, *IEEE Electron Device Lett.*, Vol. 39, Issue 12, Dec. 2018, pp. 1928–1931.
[25]. A. S. Katkar, *et al.*, Advanced Room Temperature Single-Electron Transistor of a Germanium Nanochain with Two and Multitunnel Junctions, *ACS Appl. Electron. Mater.*, Vol. 2, Issue 7, Jul. 2020, pp. 1843–1848.
[26]. G. Lientschnig, I. Weymann, P. Hadley, Simulating Hybrid Circuits of Single-Electron Transistors and Field-Effect Transistors, *Jpn. J. Appl. Phys.*, Vol. 42, Part 1, Issue 10, Oct. 2003, pp. 6467–6472.
[27]. T. Tsiolakis, G. P. Alexiou, N. Konofaos, Design and simulation of NAND gates made of single electron devices, in *Proceedings of the 12th Pan-Hellenic Conference on Informatics, PCI'2008*, 2008, pp. 131–134.
[28]. M. Hayati, M. Nouri, S. Haghiri, D. Abbott, A Digital Realization of Astrocyte and Neural Glial Interactions, *IEEE Trans. Biomed. Circuits Syst.*, Vol. 10, Issue 2, 2016, pp. 518–529.
[29]. B. Câmara, J. Guimarães, J. Camargo, Behavior Analysis of a Simultaneous Read/Write Nanoelectronic SRAM, in *Sensors & Transducers*, Vol. 227, Issue 11, November 2018, pp. 15–20.
[30]. Linear, Linear Technology - Design Simulation and Device Models, 2017. [Online]. Available: http://www.linear.com/designtools/software/#LTspice [Accessed: 28-Jan-2017].